crystals

MDPI

Article

Analytical Study of Powder Stream Geometry in Laser-Based Direct Energy Deposition Process with a Continuous Coaxial Nozzle

Qipeng Liu [1], Kun Yang [2], Yuehua Gao [1,2,*], Fencheng Liu [1], Chunping Huang [1] and Liming Ke [1]

[1] National Defense Key Disciplines Laboratory of Light Alloy Processing Science and Technology, Nanchang Hangkong University, Nanchang 330063, China; qp_liu@126.com (Q.L.); fencheng999@163.com (F.L.); cphuang@nchu.edu.cn (C.H.); limingke@nchu.edu.cn (L.K.)
[2] College of Locomotive and Rolling Stock Engineering, Dalian Jiaotong University, Dalian 116028, China; yk10140124@163.com
* Correspondence: 70956@nchu.edu.cn; Tel./Fax: +86-0791-83863735

Abstract: In the process of laser-based direct energy deposition, the particle concentration distribution and geometric characteristics of powder flow play an important role in laser–powder interaction and powder utilization, and they affect the forming quality and accuracy. In the current study, based on the geometry information of a powder nozzle and the divergence angles of a powder jet at the nozzle outlet, the geometric profile of a powder stream is analyzed. A set of formulas for calculating the geometric characteristics of the powder stream is derived based on an analytic geometry method. The influence of each parameter on the geometric characteristics of the powder stream is further studied using single-factor and sensitivity analyses. Validation is performed by comparing the results from the presented analytical expressions with those from experiments and/or simulations in published papers. The analytical formulas provided in this paper are simple and practical, providing a theoretical foundation for the control of powder flow and related processes in the forming process.

Keywords: laser-based direct energy deposition; continuous coaxial nozzle; powder stream geometry; analytical modeling

Citation: Liu, Q.; Yang, K.; Gao, Y.; Liu, F.; Huang, C.; Ke, L. Analytical Study of Powder Stream Geometry in Laser-Based Direct Energy Deposition Process with a Continuous Coaxial Nozzle. *Crystals* **2021**, *11*, 1306. https://doi.org/10.3390/cryst11111306

Academic Editors: Pan Wang, Takayoshi Nakano, Jiaming Bai and Liqun Li

Received: 19 September 2021
Accepted: 20 October 2021
Published: 27 October 2021

1. Introduction

Laser-based direct energy deposition (LDED), also referred to as laser-engineered net shaping (LENS), laser direct metal deposition (LDMD), laser metal/melting deposition (LMD), direct laser deposition (DLD), and laser cladding (LC) in various references [1–3], is a typical process of additive manufacturing (AM), and LC has been successfully used in repairing components and improving corrosion and wear resistance [4]. In these processes, the powder is usually fed into a laser-induced melt pool on the substrates by the powder delivery system with various nozzles. The nozzles are mainly classified into three categories: lateral, discontinuous coaxial (radially symmetrical), and continuous coaxial nozzles [5]. Coaxial nozzles, which allow the powder stream to flow coaxially with the laser beam, provide the capability of omnidirectional deposition and better powder efficiency. De Oliveira et al. [6] argued that continuous coaxial deposition is most suitable for the additive buildup of complex structures.

Although coaxial powder feeding has been commonly used for the deposition of various materials, there remains a lack of comprehensive understanding due to the complex physics involved, such as laser–powder–gas interactions. One of the challenging issues is the powder flow trajectories and the related distribution of the powder stream, which influences powder utilization efficiency, laser attenuation, track dimensions, and even the final quality of the product. It has been proved that the distribution of the powder stream is an important parameter that must be considered to obtain optimum conditions of the

DED [7]. Therefore, it is necessary to study this issue via experimental, numerical, and analytical investigations.

The powder stream from the nozzle usually experiences a converging, merging, and diverging process. Some authors [8–10] characterized the distribution of powder concentration based on image analysis and optical sensor methods and found that the powder distribution exhibited a Gaussian mode in the radial (transverse) and/or axial (vertical) directions. Tabernero et al. [11] attempted to distinctly identify the annular, Gaussian, and divergent zones and concluded that the Gaussian zone is the region where the laser cladding process operates well during deposition. Eisenbarth et al. [12] considered the effect of the base material in their experimental investigation. Doubenskaia et al. [13] experimentally measured the geometric quantities of the powder stream profile, including the divergence angles, waist position, waist width, and waist length.

Due to the difficulty and high cost of experimental testing, numerical simulation was developed to investigate the issue. Lin [14] modeled and solved the issue of gas–powder coupling flow using time-averaged governing equations with the standard k-ε turbulence model and additional transport equations of the powder phase, in which the particle collision and heat transfer by laser radiation were not considered. Similar modeling strategies were adopted for cases with different materials and processes [11,13,15–17]. Pan and Liou [18] considered the effect of particle collisions in modeling. Wen et al. [19] and Guan et al. [20] developed more complex models to take into account laser–powder interaction. Compared to the experimental measurement, the numerical investigation provides a more convenient and comprehensive approach to the geometric characteristics of the powder stream.

Analytical modeling is a traditional way of understanding unfamiliar aspects of a process [2]. The advantage of analytical modeling over numerical simulation lies in the simple and fast calculation, which is essential for the real-time, closed-loop control of the process [21,22]. Thus, analytical modeling was also performed by some authors in addition to experimental and numerical investigations. Lin [8] gave a Gaussian formulation of the concentration distribution in the transverse direction of the powder stream. Lin [23], Pinkerton and Li [9], Yang et al. [10], and Yang [24] gave preliminary geometric demonstrations of the powder stream and developed analytical expressions describing the powder concentration variation along the vertical direction. Existing research mainly focuses on the spatial distribution of powder concentration, while few studies have developed analytical formulation for the geometric characteristics of the powder stream, such as the focal position, waist width, and length. Moreover, there are some valuable contributions [5,25,26] to determining the characteristics of the powder stream of discontinuous coaxial nozzles, such as the concentration mode and powder stream radius, but the results are not suitable for the continuous coaxial nozzle because of the difference in the nozzle structures.

This paper presents a comprehensive study of the geometry of the powder stream in the LDED process with a continuous coaxial nozzle. The geometric relationship among the nozzle size, nozzle inclined angle, the divergence angles of the powder jet at the nozzle outlet, and the powder stream profile are analyzed in detail. Subsequently, the analytical expressions of the geometric characteristics of the powder stream are derived to estimate the position of the focal plane, the starting and ending positions of the waist region, and the waist width. The influence of each parameter on the geometric characteristics of the powder stream is further studied on the basis of analytical expressions using single-factor and sensitivity analyses. The developed formulas are applied to predict and analyze the geometric characteristics of the powder stream under some typical process parameters, and the calculation results are compared with the experimental and/or simulation results in the literature to verify the developed analytical model.

2. Analytical Expressions for the Geometric Characteristics of the Powder Stream

A schematic diagram for half of a continuous coaxial nozzle is shown in Figure 1. A laser beam passes through the central cavity of the structure, and the powder particles

are transported in the annular passage, which has a cone shape that is coaxial with the laser beam. The geometric profiles of the nozzle and the powder flow field below it at any symmetry plane are shown in Figure 2. The annular nozzle has a cone angle of θ_n relative to the laser beam center line (z-axis). The powder jet at the nozzle outlet usually diverges to a certain extent, which can be characterized by the upper and lower divergence angles θ_{p1} and θ_{p2}, respectively. Due to the interaction of gravity, the carrier gas, and the shielding gas, the divergence angles are generally small but not zero. The virtual focus of the powder jet in the nozzle is denoted as O_1 and O_2, and the upper and lower edge lines are denoted as O_1A and O_2A, and O_1B and O_2B, respectively. The powder particles ejected from the annular nozzle outlet flow down and experience a process first of convergence and then of divergence, during which a waist region with a certain width and length is formed at the central area of the laser beam.

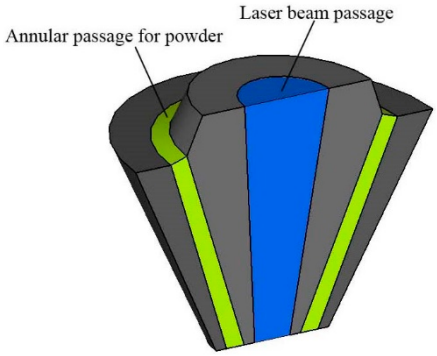

Figure 1. Schematic diagram of half of the coaxial nozzle structure.

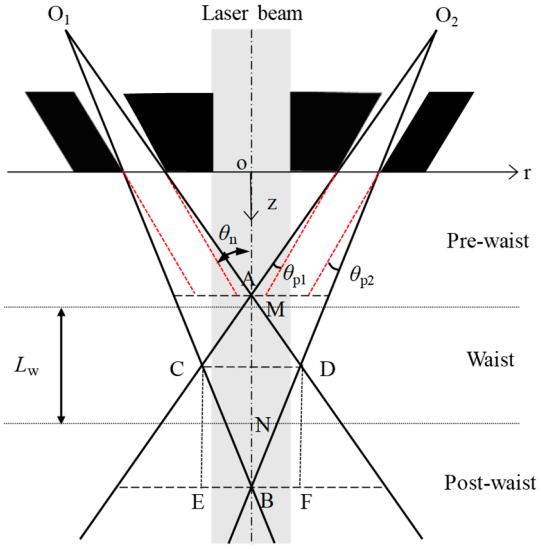

Figure 2. Geometric profile of the powder stream.

As can be seen in Figure 2, the annular powder stream gradually converges to the central area and into a circular stream at the horizontal section with point A. Then, the cross-section of the circular stream gradually narrows, and the powder concentration gradually increases. The convergence is completed at the CD plane, which can be regarded as the focal plane of the powder stream. At the CD plane, the distribution of powder particles is most concentrated. Below the CD plane, the cross-section of the powder stream gradually increases with the increase in the distance from the CD plane. On the horizontal section with point B, where the intersection of the lower edge lines of the powder jet is located, most of the particles fall outside the focus diameter, and the powder stream shows significant divergence characteristics. Most of the powder particles are concentrated near the centerline in the region between points M and N, which is called the waist region of the

powder stream [19]. According to the particle distribution characteristics on the horizontal section plane at different locations, the powder stream can be roughly divided into three stages [19], i.e., the pre-waist, waist, and post-waist stages, as shown in Figure 2.

Although the typical geometric characteristics of the powder stream have been determined in experimental tests and numerical simulations under specific process parameters, the intrinsic geometric relationship between these values and their calculation methods has not yet been revealed due to the lack of analytical analysis. Therefore, these values are only applicable to the specific processes given in the literature and cannot be widely applied. In this section, the intrinsic geometric relationship related to the powder flow and nozzle parameters is analyzed and elaborated. The analytical formulas are derived to estimate the main geometric characterization of the powder stream, including the focal plane position, waist width, and starting and ending positions of the waist region.

2.1. Focal Plane Position of the Powder Stream

The focal plane position of the powder stream is a key factor in the laser-based direct energy deposition process, which provides a basic and important reference for the determination of the optimal placement position of the substrate. It can be observed in Figure 2 that the focal plane of the powder stream is the CD plane, and its position can be indicated by the distance from the nozzle outlet to the CD plane. The local geometric diagram is enlarged for the convenience of elaboration, as shown in Figure 3. d_{In} is the inner diameter of the annular nozzle, and H is the width of the powder passage. C_1 is the intersection of O_1C and the outer wall of the powder passage, and C_2 is the intersection of O_2C and the inner wall of the powder passage. A vertical line from point C to C_1C_2 is drawn, and the vertical foot is P. The distance from the nozzle outlet to the CD plane, i.e., L_{CD}, is equal to the length of the line segment CP.

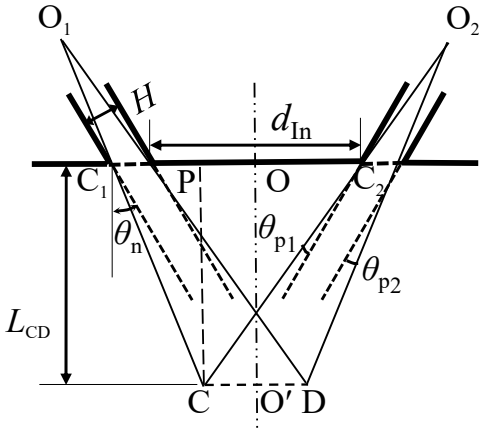

Figure 3. Local geometric demonstration for the focal plane of the powder stream.

The length of segment C_1C_2 can be expressed by the nozzle parameters as $d_{\mathrm{In}} + H/\cos\theta_{\mathrm{n}}$. It can be seen in Figure 3 that $|C_1C_2| = |C_1P| + |C_2P|$; thus, the following equation is obtained:

$$L_{\mathrm{CD}} \times \tan\angle C_1CP + L_{\mathrm{CD}} \times \tan\angle C_2CP = d_{\mathrm{In}} + H/\cos\theta_n \quad (1)$$

According to the geometric relationship shown in Figure 3, $\angle C_1CP = \theta_{\mathrm{n}} - \theta_{\mathrm{p2}}$, $\angle C_2CP = \theta_{\mathrm{n}} + \theta_{\mathrm{p1}}$. Substitution of them into Equation (1) results in the expression for L_{CD} as shown below:

$$L_{\mathrm{CD}} = \frac{d_{\mathrm{In}} + H/\cos\theta_{\mathrm{n}}}{\tan(\theta_{\mathrm{n}} - \theta_{\mathrm{p2}}) + \tan(\theta_{\mathrm{n}} + \theta_{\mathrm{p1}})} \quad (2)$$

Equation (2) is the formula for the calculation of the focal plane position. From this equation, it can be seen that the focal plane position L_{CD} is related to the inner diameter d_{In}, nozzle inclination angle θ_{n}, the width of the powder passage H, and the divergence angles of the powder jet at the nozzle outlet θ_{p1} and θ_{p2}. L_{CD} has linear relationships with

d_{In} and H and non-linear relationships with the other parameters in Equation (2). Figure 4 shows the effects of each parameter on L_{CD} when the other parameters remain constant (d_{In} = 4 mm, θ_n = 30°, H = 1.5mm, θ_{p1} = 5°, and θ_{p2} = 10°), which shows that the focal plane position changes monotonously with these parameters.

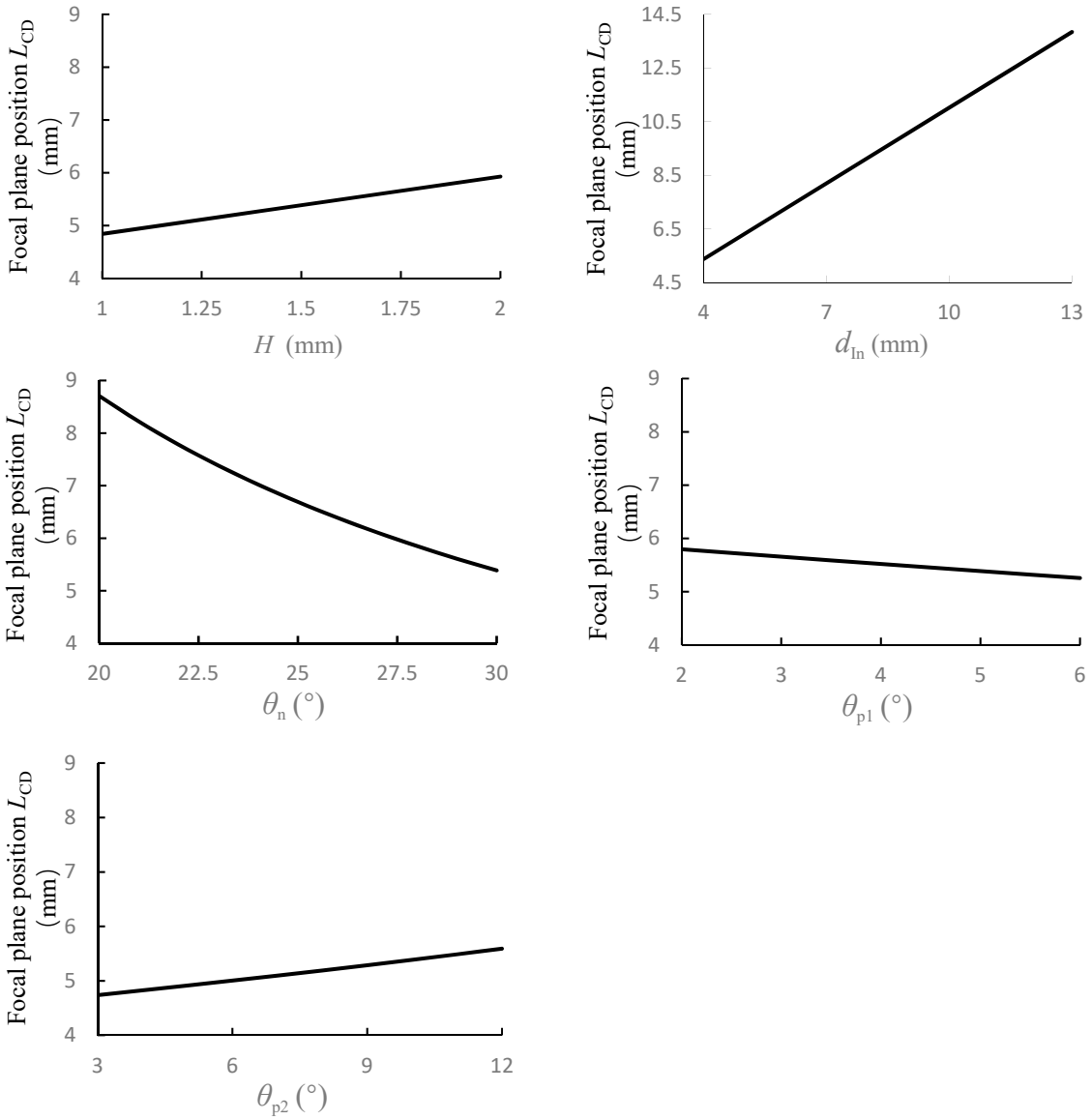

Figure 4. The effects of each parameter on the focal plane position L_{CD}.

The variables d_{In}, θ_n, and H are structural parameters of the nozzle. The focal plane position will move down if the inner diameter d_{In} of the nozzle and/or the width of the powder passage H is enlarged, while it will move up when the inclination angle θ_n of the nozzle increases. The structural parameters d_{In} and θ_n have an obvious influence on the focal plane position for the given variation ranges, while the structural parameter H has a small impact. The divergence angles θ_{p1} and θ_{p2} are both processing-related parameters, which could also affect the focal plane position. They have opposite effects on L_{CD}, and their effects are nearly linear. The focal plane position will move up if θ_{p1} increases and move down if θ_{p2} increases and a shift of about 1 mm will be caused in the given variation ranges. Thus, the focal plane position will shift when the processing parameters change even though the structural parameters are fixed.

Table 1 gives the sensitivity of L_{CD} to each parameter, which provides the quantitative characterization for the impact of unit change of each parameter. θ_n has an obvious non-

linear effect on L_{CD}, and, thus, a variation range of the sensitivity value is given. From this table, size parameters d_{In} and H are two highly sensitive factors for L_{CD}, and they have similar effects. The angle parameter θ_n is sensitive when its value is small (20°~25°), while its effect weakens when its value increases, and it has a similar effect with that of θ_{p1} when $\theta_n > 30°$. The angle parameter θ_{p2} is a slightly sensitive factor compared with θ_n and θ_{p1}.

Table 1. Sensitivity of L_{CD} to each parameter.

Parameters	d_{In}	H	θ_n	θ_{p1}	θ_{p2}
L_{CD}	0.9397	1.085	−0.4701~−0.1841(mm/○)	−0.1351(mm/○)	0.009(mm/○)

In Equation (2), the upper and lower divergence angles (θ_{p1} and θ_{p2}, respectively) of the powder jet at the nozzle outlet are considered, while their effects have been ignored in some previous works [9], and the focal plane position of the powder stream is approximately taken as the intersection point of the powder passage centerlines, i.e.,

$$L'_{CD} = \frac{d_{In} + H/\cos\theta_n}{2\tan\theta_n} \tag{3}$$

$L_{CD} \neq L'_{CD}$ from Equations (2) and (3), which means that the focal plane position of the powder stream is no longer at the intersection of the powder passage centerlines when considering the divergence of the powder jet at the nozzle outlet, which is consistent with the conclusion in [12]. $L_{CD} = L'_{CD}$ only when $\theta_{p1} = \theta_{p2} = 0$. Nevertheless, the fact is that the divergence angle of the powder jet is usually not zero due to the influence of gravity combined with inner/outer shielding gas, and the upper divergence angle is generally less than or equal to the lower divergence angle, i.e., $\theta_{p1} \leq \theta_{p2}$ [13,15]. The effects of divergence angles are discussed in detail below.

The difference between Equations (2) and (3) lies in the denominator, and it can be expressed as follows:

$$\begin{aligned} \Delta &= \tan(\theta_n - \theta_{p2}) + \tan(\theta_n + \theta_{p1}) - 2\tan\theta_n \\ &= \sec^2\theta_n(\theta_{p1} - \theta_{p2}) + \sec^2\theta_n \tan\theta_n\left(\theta_{p1}^2 + \theta_{p2}^2\right) + o\left(\theta_{p1}^2\right) \end{aligned} \tag{4}$$

If $\theta_{p1} = \theta_{p2} = \theta_p \neq 0$, the relative error δ can be expressed as

$$\delta = \Delta/(2\tan\theta_n) = \sec^2\theta_n(\theta_p^2) \tag{5}$$

Equation (5) shows that the relative error is a function of the quadratic term of the divergence angle. According to references [13,16,17,19,20], the value of θ_n usually lies in the range of 20°~30°. If θ_n = 30°, we have $\delta = 1.33\theta_p^2$; the curve of δ versus θ_p is shown in Figure 5.

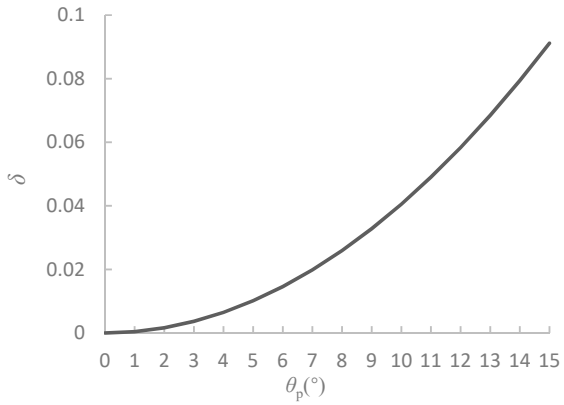

Figure 5. δ versus θ_p when upper and lower divergence angles are consistent.

It can be seen in Figure 5 that $\delta \leq 0.01$ when $\theta_p \leq 5°$. That is, the difference between Equations (2) and (3) is negligible when the divergence angle is less than 5°, and the focal plane position of the powder stream is very close to the intersection position of the powder passage centerlines. When $\theta_p > 5°$, the difference between the two shows a non-linear increasing trend with the increase in the divergence angle.

When $\theta_{p1} \neq \theta_{p2}$, the relative error δ can be expressed as follows:

$$\begin{aligned} \delta &= \delta_1 + \delta_2 \\ &= \frac{1}{\sin 2\theta_n}(\theta_{p1} - \theta_{p2}) + \frac{1}{2}\sec^2\theta_n\left(\theta_{p1}^2 + \theta_{p2}^2\right) \end{aligned} \tag{6}$$

Substitution of $\theta_n = 30°$ into Equation (6) gives

$$\delta = \delta_1 + \delta_2 = 1.15(\theta_{p1} - \theta_{p2}) + 0.67\left(\theta_{p1}^2 + \theta_{p2}^2\right) \tag{7}$$

The surface of δ versus θ_{p1} and θ_{p2} is shown in Figure 6.

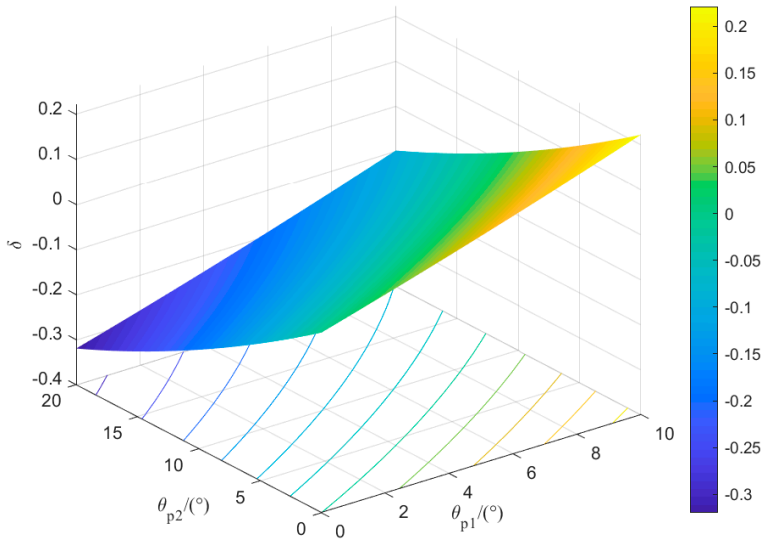

Figure 6. Change in δ with the upper and lower divergence angles.

From Equations (6) and (7) and Figure 6, when $\theta_{p1} \neq \theta_{p2}$, the relative error is not only related to the values of θ_{p1} and θ_{p2} but also to the difference between them. Besides, since $\delta_1 < 0$ and $\delta_2 > 0$, the value of δ may be positive, negative, or zero. If δ is positive, $L_{CD} < L'_{CD}$; the focal plane of the powder stream is located above the intersection of the powder passage centerlines. If δ is negative, $L_{CD} > L'_{CD}$; the focal plane of powder stream is located below the intersection of the powder passage centerlines. Especially, if δ is zero, $L_{CD} = L'_{CD}$; the focal plane position of the powder stream coincides with the intersection point of the powder passage centerlines.

In this subsection, the formula for calculating the focal plane position of the powder stream is derived considering the analytic geometry approach, and the relationship between the focal plane position and the intersection of the powder passage centerlines is comprehensively analyzed, which provides a theoretical reference for the understanding and determination of the focal plane position of the powder stream.

2.2. Waist Width of the Powder Stream

The prediction of the waist width is useful for the prediction of the track width and for the selection and adjustment of the laser spot size. According to the geometric relationship shown in Figure 2, the length of the segment CD can be expressed as follows:

$$|CD| = 2|CO'| = 2|PO| = 2(|C_1O| - |C_1P|) \tag{8}$$

The length of segment C_1O is equal to $(d_{In}/2 + H/\cos\theta_n)$, and the length of segment C_1P is equal to $[L_{CD} \times \tan(\theta_n - \theta_{p2})]$. Substitution of them into Equation (8) results in

$$|CD| = d_{In} + \frac{2H}{\cos\theta_n} - 2L_{CD} \times \tan(\theta_n - \theta_{p2}) \quad (9)$$

According to the discussion in reference [19], the waist width d_w of the powder stream is defined as the size of the area where the powder has a high concentration (higher than a certain value) rather than where all particles coverage. Thus, the waist width should be expressed as

$$d_w = \alpha_w |CD| \quad (10)$$

in which the coefficient α_w can be determined from the powder distribution in the cross-section. The powder distribution in the waist region follows Gaussian distribution [8], thus the concentration can be described as

$$C(r) = C_m \exp\left(\frac{-r^2}{2\sigma^2}\right) \quad (11)$$

where C_m is the maximum powder concentration at the center of the stream, σ is a parameter characterizing the powder stream range, and r denotes the radius from the center.

The waist width is defined here as the radius with which the powder concentration decreases to $1/e^2$ of the maximum value, and it can be determined from Equation (11) that

$$(d_w)_{C=C_m/e^2} = 2 \times r|_{C(r)=C_m/e^2} = 4\sigma \quad (12)$$

According to Equation (12), 86.5% of the powder particles lie in the waist width range.

The CD range should contain all of the powder particles in Figure 3. However, the length of CD satisfying this condition is infinite, according to Equation (11). Therefore, an approximate treatment is needed in the calculation process. The radius corresponding to the CD range is assumed as the position where the powder concentration decreases to 10^{-5} C_m (99.999% of the powder particles lie in the range). It can be determined from Equation (11) that

$$(|CD|)_{C=10^{-5}C_m} = 2 \times r|_{C(r)=10^{-5}C_m} = 9.6\sigma \quad (13)$$

By use of Equations (10), (12), and (13), the following is obtained:

$$\alpha_w = \frac{(d_w)_{C=C_m/e^2}}{(|CD|)_{C=C_m 10^{-5}}} = \frac{4\sigma}{2\sqrt{10\ln 10}\sigma} = 0.417 \quad (14)$$

Then, Equation (10) can be rewritten as

$$d_w = 0.417|CD| = 0.417\left[d_{In} + \frac{2H}{\cos\theta_n} - 2L_{CD} \times \tan(\theta_n - \theta_{p2})\right] \quad (15)$$

Equation (15) is the final expression for the waist width of the powder stream. From this equation, the waist width d_w is also related to the nozzle inner diameter d_{In}, the nozzle inclination angle θ_n, the powder passage width H, and the divergence angles θ_{p1} and θ_{p2}. Figure 7 shows the effects of each parameter on d_W when other parameters remain constant (d_{In} = 4 mm, θ_n = 30°, H = 1.5 mm, θ_{p1} = 5°, θ_{p2} = 10°), which shows that waist width also changes monotonously with these parameters.

The waist width will increase if the diameter of the nozzle inner and/or the powder passage width are enlarged, while it will non-linearly decrease when the nozzle inclination angle increases. The structural parameters d_{In} and H have an obvious influence on the waist width for the given variation ranges, while the structural parameter θ_n has a minimal impact. The divergence angles θ_{p1} and θ_{p2} have nearly linear effects on the waist width, and the waist width will increase if θ_{p1} and/or θ_{p2} increase. The changes in θ_{p1} and θ_{p2} could cause a change of about 0.5 mm on waist width, in which θ_{p2} will contribute more

as it has a greater impact than that of θ_{p1} for the given variation ranges. Thus, the waist width could be affected by both structural and processing parameters.

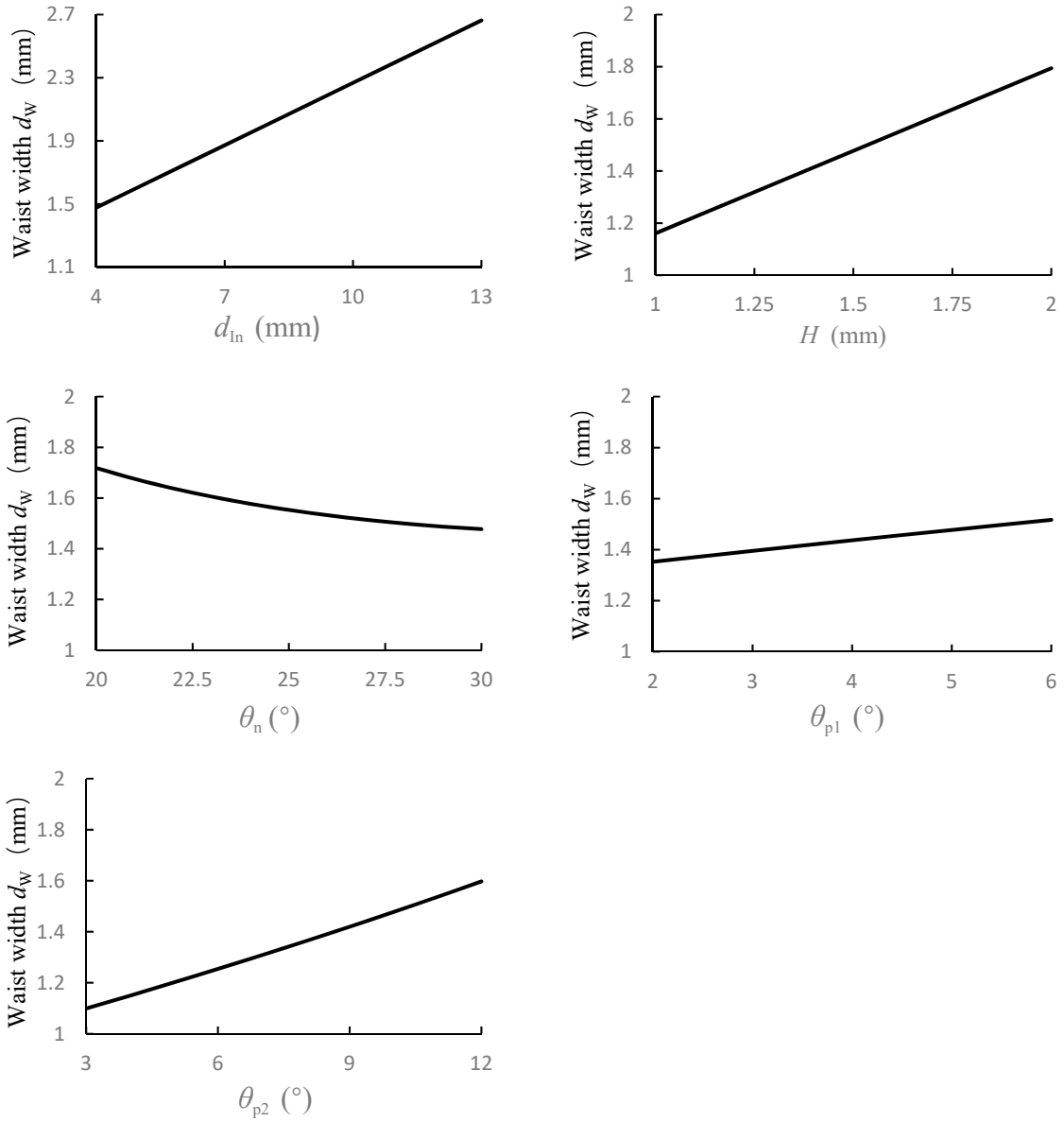

Figure 7. The effects of each parameter on the waist width d_W.

Table 2 shows the sensitivity of d_W to each parameter. For the size parameters, H is a highly sensitive factor for d_W, while d_{In} is slightly sensitive. For the angle parameters, θ_n has a similar effect on d_W with that of θ_{p1} and θ_{p2} when its value is near 20°, and the effect weakens when its value increases. It means that the influence of θ_n is less than that of θ_{p1} and θ_{p2} when $\theta_n > 20°$.

Table 2. Sensitivity of d_W to each parameter.

Parameters	d_{In}	H	θ_n	θ_{p1}	θ_{p2}
d_W	0.1313	0.6336	−0.0503~−0.0193(mm/°)	0.041(mm/°)	0.0553(mm/°)

2.3. Starting and Ending Positions of the Waist Region

The prediction of the starting and ending positions of the waist region is mainly used to determine the Gaussian distribution region of the powder concentration, thus as to determine the region where the substrate should be placed. Placing the substrate in the Gaussian distribution region can ensure powder utilization and forming quality [5,11]. It is suggested in [19] that the starting point of the waist region should be defined as the position where the powder flow begins to merge, the powder concentration is Gaussian distribution relative to the centerline of the powder stream, and the ending point is defined as the position where the powder begins to diverge, and its concentration no longer shows obvious Gaussian distribution. According to the definition, the analytical formulas for the starting and ending positions of the waist region are proposed and derived here.

As shown in Figure 2, the starting point M usually does not coincide with point A but is a certain distance below point A, because the particle concentration on the cross-section with point A does not show an obvious Gaussian distribution. Similarly, the ending point N of the waist region is not coincident with point B but a certain distance above point B, because the powder distribution exhibits significant divergence on the cross-section with point B.

It is adopted here that the starting point M of the waist region is located at the intersection of the bisector of upper divergence angle and the nozzle central axis (OB), and the ending point N is located at the intersection of the bisector of lower divergence angle and the nozzle central axis (OB), as shown in Figure 8. The specific positions of M and N can be determined by the corresponding geometric relationship in Figure 8. The lengths of segments OM and ON are computed by

$$L_{OM} = \frac{|\mathrm{OA}'|}{\tan \angle \mathrm{A}'\mathrm{MO}} = \frac{d_{\mathrm{In}}/2}{\tan(\theta_n + \theta_{\mathrm{p1}}/2)} \tag{16}$$

$$L_{ON} = \frac{|\mathrm{OC}_1|}{\tan \angle \mathrm{C}_1\mathrm{NO}} = \frac{d_{\mathrm{In}}/2 + H/\cos\theta_{\mathrm{n}}}{\tan(\theta_n - \theta_{\mathrm{p2}}/2)} \tag{17}$$

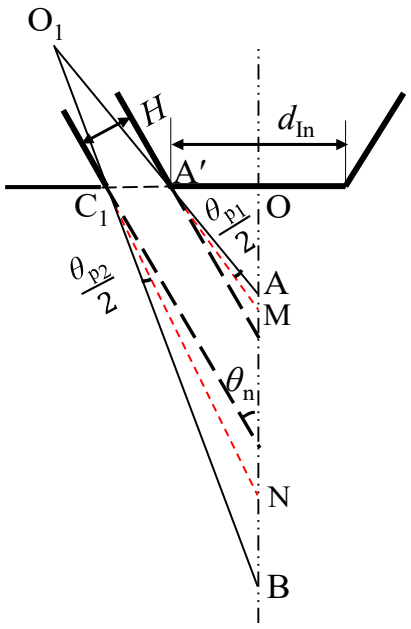

Figure 8. Geometric diagram of starting and ending positions of the waist zone.

The starting position of the waist region has no relationship with the width of the powder passage H and/or the lower divergence angle θ_{p2}, and the ending position of the waist region has no relationship with the upper divergence angle θ_{p1} in Equation (16).

Figure 9 shows the effects of each parameter on segments OM and ON when other the parameters remain constant (d_{In} = 4 mm, θ_n = 30°, H = 1.5 mm, and θ_{p1} = 5°, θ_{p2} = 10°). From Figure 9, the starting and ending points of the waist region will both move down with the increase in the inner diameter d_{In}, and the length of the waist region will increase linearly. The starting and ending points of the waist region will both move up with the increase of the θ_n, and the length of the waist region will decrease non-linearly. The starting point of the waist region will move up with the increase in the upper divergence angle θ_{p1}, while the movement amount is small. The ending point of the waist region will move down with the increase in the width of the powder passage H and lower divergence angle θ_{P2}, and the length of the waist region will increase linearly.

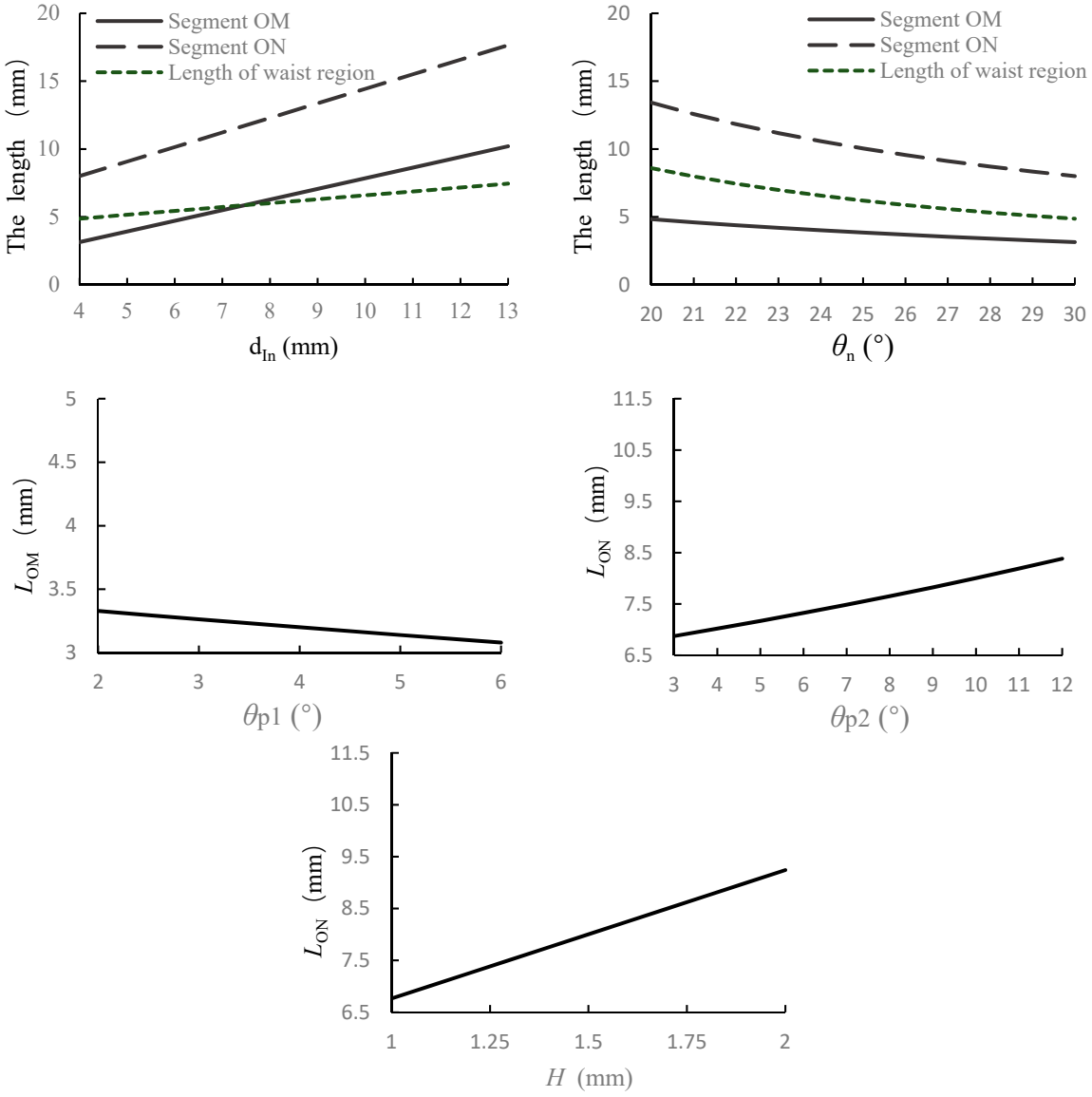

Figure 9. The effects of each parameter on L_{OM} and L_{ON}.

Table 3 gives the sensitivity of L_{OM} and L_{ON} to each parameter. For the starting point of the waist region L_{OM}, the size parameter d_{In} is a highly sensitive factor. The angle parameter θ_n is a moderately sensitive factor for L_{OM}, and θ_{p1} is a slightly sensitive factor. For the ending point of the waist region L_{ON}, the size parameters H and d_{In} are both highly sensitive factors. The angle parameter θ_n is a highly sensitive factor when its value is small (θ_n < 25°), and its effect weakens when the value increases. The angle parameter θ_{p2} is also a moderately sensitive factor for L_{ON}.

Table 3. Sensitivity of L_{OM} and L_{ON} to each parameter.

Parameters	d_{In}	H	θ_n	θ_{p1}	θ_{p2}
L_{OM}	0.7848	—	−0.2232~−0.1092 (mm/°)	−0.0622 (mm/°)	—
L_{ON}	1.0723	2.4763	−0.8~−0.264 (mm/°)	—	0.1673 (mm/°)

In this section, some analytical expressions for the geometric characteristics of the powder stream are derived, and they are usable when the collision effect between powder particles is weak, which is a commonly used assumption in process modeling and simulation [5,9–17,19,20]. Moreover, these analytical expressions can be used on the basis of that the divergence angles θ_{p1} and θ_{p2} are given. Processing-related parameters θ_{p1} and θ_{p2} have complicated relationships with processing parameters, and this issue is not discussed in this paper.

The influence of each parameter on the geometric characteristics of the powder stream was comprehensively analyzed based on the analytical expressions. From Tables 1–3, structural parameters H and d_{In} are two key factors affecting the powder stream. The structural parameter θ_n has moderately sensitive effects on L_{CD}, L_{OM}, and L_{ON}, and a slightly sensitive effect on d_W. Processing-related parameters θ_{p1} and θ_{p2} have moderately sensitive effects on L_{CD} and L_{ON}, respectively, and they have slightly sensitive effects on d_W and L_{OM}.

3. Examples for Verification

In this section, three experimental and/or simulation examples are used to verify the derived analytical expressions.

Example 1: In reference [19], the structure of a continuous coaxial powder stream under typical nozzle and process parameters was simulated in detail, and the specific values of the geometric characteristics were given. The powder used was Stellite 6 with a density of 8380 kg/m3. The particle shape was quasi-spherical, and the particle size range was 45–150 μm. The powder feeding rate was 3 g/min. According to the parameters and results given in the reference, the basic parameters can be calculated and acquired. The inner nozzle diameter was 9.14 mm, and the horizontal width of the powder passage at the nozzle outlet was 1.2 mm. The inclination angle of the powder passage was 25°, and the upper and lower divergence angles at the nozzle outlet were about 4° and 9°, respectively. The velocity of the carrying gas and inner shielding gas was 2 m/s and 1.2 m/s, respectively. The comparison between the calculated values using the analytical formulas developed in this paper and the simulation values given in reference [19] is shown in Table 4.

Table 4. Comparison of analytical and numerical results.

	L_{CD}	d_w	L_{OM}	L_{ON}
Analytical results (mm)	12.29	2	8.97	15.43
Simulation results [19] (mm)	12	1.87	9	18
Relative error (%)	2.4	6.9	0.3	14.3

Comparing the results in Table 4, it can be seen that the analytical prediction results are highly consistent with the simulation results for the focal plane position, waist width, and starting position of the waist region, which shows the validity of the presented analytical formulas in this paper. For the ending position of the waist region, the difference between the analytical value and the simulation value was slightly larger, and the relative error was 14.3%. The analytical prediction value was lower than the simulation value, which shows that the analytical prediction results are more conservative.

Example 2: The geometric characteristics of a continuous coaxial powder stream with different nozzle diameters and inclination angles were analyzed using experimental tests and numerical simulation in [13]. The powder used was Inconel 718, with a density of

8190 kg/m^3. The particle shape was quasi-spherical, and the size range was 50–150 μm. The powder feeding rate was 18 g/min. Other process parameters are listed in Table 5.

Table 5. The process parameters in [13].

No.	Horizontal Width of Powder Passage/(mm)	Inner Nozzle Diameter/(mm)	Nozzle Inclination Angle θ_n/(°)	Inner Shielding Gas Velocity/(m/s)	Carrying Gas Velocity/(m/s)	Upper Divergence Angle θ_{p1}/(°)	Lower Divergence Angle θ_{p2}/(°)
1	1.0	10	25	1.06	4.34	5 ± 0.5	20 ± 0.5
2	1.0	13	32	0.63	3.41	8 ± 0.5	22 ± 0.5

Table 6 shows a comparison among the analytical results, the simulation, and the experimental results in reference [13] for the focal plane position of the powder stream. The predicted values of the analytical formula were close to the simulation values in the literature, which indicates the rationality and effectiveness of the analytical formula. The collision effect between powder particles was significant in this example due to the high powder feeding rate (up to 18 g/min). Therefore, the deviation between the analytical/simulation results and the experimental results was relatively larger, which is due to the fact that the particle collision effect was not considered in the analytical and/or numerical models [13,15–17,19,20].

Table 6. Comparison of results for the focal plane position L_{CD}.

No.	Analytical Results (mm)	Simulation Results [13] (mm)	Experimental Results [13] (mm)
1	16.5 ± 0.5	14.8 ± 0.3	9.1 ± 0.3
2	13.8 ± 0.3	14.0 ± 0.2	9.3 ± 0.3

Table 7 gives the comparison of waist width between the analytical and experimental values in [13]. It can be seen that the analytical prediction results were in good agreement with the experimental results. These results show that the particle collision effect has a weak effect on the waist width.

Table 7. Comparison of results for the waist width d_W.

No.	Analytical Results (mm)	Experimental Results [13] (mm)
1	3.5 ± 0.1	3.4 ± 0.3
2	3.9 ± 0.1	3.9 ± 0.3

Example 3: In reference [17], the powder flow of laser cladding with a continuous coaxial nozzle was simulated. The powder used was NiCoCrAlY, and the particle size range was 45–125 μm. The powder feeding rate was 4.2 g/min, and the velocity of the carrying gas was 0.73 m/s. The inner and outer shielding gas rates were 5.01 m/s and 1.07 m/s, respectively. The diameter of the inner nozzle d_{In} was 6 mm. The width and inclined angle of the powder passage were 2.2 mm and 30°, respectively. The divergence angles of the powder jet at the nozzle outlet were not clearly stated in reference [17], thus the divergence angles were estimated here in light of some theoretical formulas in reference [25] and existing results in similar cases [4,13,19]. With consideration of the specific conditions in reference [17], the estimated ranges of divergence angles θ_{p1} and θ_{p2} were [0°, 4°] and [4°, 10°], respectively.

The focal plane position and the starting and ending positions of the waist region were calculated based on the estimated ranges of θ_{p1} and θ_{p2}. A comparison between the analytical results and the simulation results in reference [17] is shown in Table 8. The

analytical prediction results were in good agreement with the simulation results, which confirms the validity of the analytical formula developed in this paper.

Table 8. Comparison of analytical and simulation results in [17].

	L_{CD}	L_{OM}	L_{ON}
Analytical results (mm)	7.3~8.3	4.8~5.2	10.4~12
Simulation results [17] (mm)	7.9	5	12.5

4. Conclusions

In this paper, the geometric characteristics of a continuous coaxial powder stream in laser direct energy deposition are comprehensively studied. Based on a detailed analysis of the geometric relationship, some important analytical expressions of the geometric characteristics of the powder stream, such as the focal plane position, the starting and ending positions of the waist, and the waist width, are derived without the consideration of the collision effect of powder particles. The influence of the divergence angle of the powder jet at the nozzle outlet on the position of the focal plane is analytically discussed, and the results show that the focal plane position could be affected by divergence angles of the powder jet and may be above or below the intersection of the powder passage centerlines due to different divergence angles.

The influence of each parameter on the geometric characteristics of the powder stream is further studied on the basis of the analytical expressions using single-factor and sensitivity analyses. The powder passage width and inner nozzle diameter are two essential factors affecting the powder stream. The inclination angle of the annular nozzle has moderately sensitive effects on the focal plane position and the starting and ending points of the waist region and slightly sensitive effects on the waist width. The upper and lower divergence angles have moderately sensitive effects on the focal plane position and ending point of the waist region, respectively, and they have slightly sensitive effects on the waist width and starting point of the waist region.

The developed formulas are applied to predict the stream geometry in typical deposition processes, and the results are compared to the experimental and/or simulation results in the literature. The comparison shows that the presented analytical formulas have good prediction performance and are suitable for the cases in which the collision effect of powder particles is not significant. Moreover, these comparison results show that the particle collision effect has a remarkable influence on the focal plane position and a weak influence on the waist width.

Future research will be devoted to considering the effect of powder collision in the analytical prediction formula and determining the divergence angles of the powder jet at the nozzle outlet based on theoretical and/or numerical approaches.

Author Contributions: Conceptualization, Q.L.; methodology, Q.L. and K.Y.; investigation, Q.L., K.Y., Y.G. and F.L.; writing—original draft preparation, Q.L.; writing—review and editing, Q.L., Y.G., C.H. and L.K.; visualization, K.Y.; supervision, Y.G. All authors have read and agreed to the published version of the manuscript.

Funding: National Natural Science Foundation of China, grant number 51865036. The Natural Science Foundation of Jiangxi Province, grant number 20192ACBL21050.

Data Availability Statement: All the data presented and/or analyzed in this study are available upon request from the corresponding author.

Conflicts of Interest: The authors declare no potential conflict of interest with respect to the research, authorship, and/or publication of this article.

References

1. Yan, Z.; Liu, W.; Tang, Z.; Liu, X.; Zhang, N.; Li, M.; Zhang, H. Review on thermal analysis in laser-based additive manufacturing. *Opt. Laser Technol.* **2018**, *106*, 427–441. [CrossRef]
2. Pinkerton, A.J. Advances in the modeling of laser direct metal deposition. *J. Laser Appl.* **2015**, *27*, S15001. [CrossRef]
3. Thompson, S.M.; Bian, L.; Shamsaei, N.; Yadollahi, A. An overview of direct laser deposition for additive manufacturing; Part I: Transport phenomena, modeling and diagnostics. *Addit. Manuf.* **2015**, *8*, 36–62. [CrossRef]
4. Toyserkani, E.; Khajepour, A.; Corbin, S. *Laser Cladding*; CRC Press: New York, NY, USA, 2005.
5. Zekovic, S.; Dwivedi, R.; Kovacevic, R. Numerical simulation and experimental investigation of gas-powder stream from radially symmetrical nozzles in laser-based direct metal deposition. *Int. J. Mach. Tools Manuf.* **2007**, *47*, 112–123. [CrossRef]
6. De Oliveira, U.; Ocelik, V.; De Hosson, J.T.M. Analysis of coaxial laser cladding processing conditions. *Surf. Coat. Technol.* **2005**, *197*, 127–136. [CrossRef]
7. Liu, J.; Li, L. Effects of powder concentration distribution of fabrication on thin-wall parts in coaxial laser cladding. *Opt. Laser Technol.* **2005**, *37*, 287–292. [CrossRef]
8. Lin, J. Concentration mode of the powder stream in coaxial laser cladding. *Opt. Laser Technol.* **1999**, *31*, 251–257. [CrossRef]
9. Pinkerton, A.J.; Li, L. Modelling powder concentration distribution from a coaxial deposition nozzle for laser-based rapid tooling. *J. Manuf. Sci. Eng.* **2004**, *126*, 33–41. [CrossRef]
10. Yang, X.; Lei, J.; Liu, Y.; Wang, Y. Experimental measurement of metal powder stream concentration field in laser manufacturing. *Chin. J. Lasers* **2006**, *33*, 993–997.
11. Tabernero, I.; Lamikiz, A.; Ukar, E.; De Lacalle, L.L.; Angulo, C.; Urbikain, G. Numerical simulation and experimental validation of powder flux distribution in coaxial laser cladding. *J. Mater. Process. Technol.* **2010**, *210*, 2125–2134. [CrossRef]
12. Eisenbarth, D.; Esteves, P.B.E.; Wirth, F.; Wegener, K. Spatial powder stream measurement and efficiency prediction for laser direct metal deposition. *Surf. Coat. Technol.* **2019**, *362*, 397–408. [CrossRef]
13. Doubenskaia, M.; Kulish, A.; Sova, A.; Petrovskiy, P.; Smurov, I. Experimental and numerical study of gas-powder flux in coaxial laser cladding nozzles of Precitec. *Surf. Coat. Technol.* **2021**, *406*, 126672. [CrossRef]
14. Lin, J. Numerical simulation of the focused powder streams in coaxial lasser cladding. *J. Mater. Process. Technol.* **2000**, *105*, 17–23. [CrossRef]
15. Jin, X.; Yang, X.; Feng, L.; Wang, Y. Numerical simulation of coaxial powder flow with carrying gas in laser manufacturing. *Chin. J. Mech. Eng.* **2007**, *43*, 161–166. [CrossRef]
16. Zhang, A.; Li, D.; Zhou, Z.; Zhu, G.; Lu, B. Numerical simulation of powder stream field on coaxial powder nozzle in laser metal direct manufacturing. *Int. J. Adv. Manuf. Technol.* **2010**, *49*, 853–859. [CrossRef]
17. Liu, H.; He, X.; Yu, G.; Wang, Z.; Li, S.; Zheng, C.; Ning, W. Numerical simulation of powder transport behavior in laser cladding with coaxial powder feeding. *Sci. China Phys. Mech. Astron.* **2015**, *58*, 104701. [CrossRef]
18. Pan, H.; Liou, F. Numerical simulation of metallic powder stream in a coaxial nozzle for the laser aided deposition process. *J. Mater. Process. Technol.* **2005**, *168*, 230–244. [CrossRef]
19. Wen, S.Y.; Shin, Y.C.; Murthy, J.Y.; Sojka, P.E. Modeling of coaxial powder stream for the laser direct deposition process. *Int. J. Heat Mass Transf.* **2009**, *52*, 5867–5877. [CrossRef]
20. Guan, X.; Zhao, Y.F. Numerical modeling of coaxial powder stream in laser-powder-based directed energy deposition process. *Addit. Manuf.* **2020**, *34*, 101226. [CrossRef]
21. Huang, Y.; Khamesee, M.B.; Toyserkani, E. A comprehensive analytical model for laser powder-fed additive manufacturing. *Addit. Manuf.* **2016**, *12*, 90–99. [CrossRef]
22. Fathi, A.; Khajepour, A.; Toyserkani, E.; Durali, M. Clad height control in laser solid freeform fabrication using a feed forward PID controller. *Int. J. Adv. Manuf. Technol.* **2006**, *35*, 280–292. [CrossRef]
23. Lin, J. Laser attenuation of the focused powder streams in coaxial laser cladding. *J. Laser Appl.* **2000**, *12*, 28–33. [CrossRef]
24. Yang, N. Concentration model based on movement model of powder stream in coaxial laser cladding. *Opt. Laser Technol.* **2009**, *41*, 94–98. [CrossRef]
25. Fu, Y.; Martin, B.; Loredo, A. Velocity distribution of the powder particles in laser cladding. *Chin. J. Lasers* **2002**, *B11*, 469–474.
26. Meriaudeau, F.; Truchetet, F. Control and optimization of the laser cladding process using matrix cameras and image processing. *J. Laser Appl.* **1996**, *8*, 317–324. [CrossRef]